J. Fluid Mech. (1995), *vol.* 299, *pp.* 133–152

A gun tunnel investigation of hypersonic free shear layers in a planar duct

By D. R. BUTTSWORTH,[1,2] R. G. MORGAN[1] AND T. V. JONES[2]

[1] Department of Mechanical Engineering, University of Queensland, Queensland 4072, Australia

[2] Department of Engineering Science, University of Oxford, Parks Road, Oxford OX1 3PJ, UK†

(Received 13 September 1994 and in revised form 12 April 1995)

An experimental investigation of high Mach number free shear layers has been undertaken. The experiments were performed using a Mach 7 gun tunnel facility and a planar duct with injection from the base of a central strut producing a Mach 3 flow parallel to the gun tunnel stream. This configuration is relevant to the development of efficient scramjet propulsion, and the gun tunnel Mach number is significantly higher than the majority of previous supersonic turbulent mixing layer investigations reported in the open literature. Schlieren images and Pitot pressure measurements were obtained at four different convective Mach numbers ranging from 0 to 1.8. Only small differences between the four cases were detected, and the relatively large high-speed boundary layers at the trailing edge of the struct injector appear to strongly influence the shear layer development in each case. The Pitot pressure measurements indicated that, on average, the free shear layers all spread into the Mach 3 stream at an angle of approximately 1.4°, while virtually no spreading into the Mach 7 stream was detected until all of the low-speed stream was entrained. The free shear layers were simulated using a PNS code; however, the experimentally observed degree of spreading rate asymmetry could not be fully predicted with the k–ϵ turbulence model, even when a recently proposed compressibility correction was applied.

1. Introduction

Over recent years research into the mixing of two streams under supersonic conditions has been driven largely by a renewed interest in the development of scramjet-powered vehicles. The air flow entering a scramjet (supersonic combustion ramjet) is maintained at a supersonic velocity throughout the duct, and fuel enters the engine through sonic or supersonic injection ports which are usually directed at some angle downstream. Because the residence time of the fuel and air is very short, combustion must occur rapidly in order to generate thrust. However, as the mixing rate of fuel and air is inherently low under supersonic conditions, the mixing process could severely limit the efficiency of the scramjet cycle.

In order to control and enhance supersonic mixing, an understanding of the characteristics and processes involved must be developed. To address fundamental issues associated with supersonic mixing, configurations involving two nominally parallel streams brought together at the trailing edge of a splitter plate are frequently studied. Numerous analytical investigations (e.g. Sandham & Reynolds 1990; Tang, Komerath & Sankar 1990; Drummond, Carpenter & Riggins 1991) and experimental studies (e.g. Chinzei *et al.* 1986; Papamoschou & Roshko 1988; Goebel & Dutton

† Address for correspondence

1991; Elliott, Samimy & Arnette 1992; Clemens & Mungal 1995) of such supersonic mixing layers have recently been conducted. The observation that mixing under supersonic conditions generally occurs more slowly than under subsonic conditions has been noted for many years (Birch & Eggers 1973) and was widely attributed to density changes which accompanied the supersonic conditions. However, Brown & Roshko (1974) demonstrated that the reduced spreading of mixing layers under supersonic conditions could not be attributed to density effects alone and so postulated the existence of a true compressibility effect.

To correlate the effects of compressibility, Bogdanoff (1983) and Papamoschou & Roshko (1988) introduced a parameter now known as the convective Mach number, M_c which theoretically was the Mach number of the supposed large-scale structures in the mixing layer, relative to the free streams. When the ratio of specific heats of the two streams which form the mixing layers are equal, the convective Mach number may be written as

$$M_c = \frac{u_1 - u_2}{a_1 + a_2}, \tag{1}$$

where u is the velocity, a is the speed of sound, and subscripts 1 and 2 refer to conditions in the primary (higher speed) and secondary (lower speed) free streams.

A measure of success in correlating the spreading rate data from various compressible mixing layers has been achieved using the convective Mach number (Samimy & Elliott 1990; Hall, Dimotakis & Roseman 1993). As the convective Mach number increases, a monotonic decrease in the compressible spreading rate, δ'_c, relative to the spreading rate of an incompressible mixing layer, δ'_i, with the same velocity and density ratio is observed. Above a convective Mach number of approximately 1, the normalized growth rate, δ'_c/δ'_i levels off to a value around 0.3, depending to some extent on the chosen correlation for δ'_i. A reduction in the extent of the turbulent activity with increased levels of compressibility (i.e. with higher convective Mach numbers), has also been observed in compressible mixing layers (Elliott & Samimy 1990; Goebel & Dutton 1991). Stability analyses performed two decades ago (Gropengiesser, 1970; Blumen, Drazin & Billings 1975), and more recently (Zhuang, Kubota & Dimotakis 1988), lend credence to the convective Mach number concept, since it has been noted (Papamoschou & Roshko 1988) that terms which implicitly involve the convective Mach number occur naturally in linear stability analyses. In addition, it has been shown that the correlation of experimental mixing layer growth trends with M_c can be emulated through stability calculations (Sandham & Reynolds 1990; Zhuang *et al.* 1988).

However, under conditions of high compressibility, the validity and utility of the convective Mach number concept appears doubtful. In the original formulation of the convective Mach number concept, the presence of two-dimensional large-scale structures, and the absence of shock waves within compressible mixing layers was assumed. Two-dimensional large-scale structures have been observed in supersonic mixing layers by Chinzei *et al.* (1986) and Clemens & Mungal (1992), but only at lower compressibility conditions. As compressibility effects become significant (values of M_c higher than approximately 0.5), both experiments (Clemens & Mungal 1992; Elliott *et al.* 1992) and theoretical work (Sandham & Reynolds 1990; Ragab & Wu 1989) indicate that the spanwise structure of the layer becomes three-dimensional and less coherent. For compressible mixing layers, the assumption of shock-free mixing also appears erroneous. If the relative speed of structures within a mixing layer is transonic, then localized weak shocks may be formed within the shear layer (Dimotakis 1991); for

supersonic convection velocities, more substantial shocks which propagate into the free stream have been observed (Hall *et al.* 1993).

Deficiencies in the use of the convective Mach number as a compressibility parameter have also been found by various theoretical and experimental studies. Using a Navier–Stokes solution, Tang *et al.* (1990) calculated the convective velocity based on the evolution of vorticity contours, and found significant discrepancies between the resulting values and those obtained using a convective Mach number approach. Sandham & Reynolds (1990) attributed the divergence of their peak amplification linear stability results for $M_c > 0.8$ to second-order compressibility effects not accounted for by the convective Mach number. Experimentally, structures within the mixing layers are generally found to convect at velocities differing widely from the theoretical convective Mach number predictions (Papamoschou 1991; Samimy, Reeder & Elliot 1990; Hall *et al.* 1993), particularly for values of M_c higher than approximately 0.5. Finally, Erdos *et al.* (1992) found that their hypervelocity mixing layers spread into the lower-speed stream at a much higher rate than was apparent on the high-speed side. Thus, they suggested that the correlation of a single value of spreading rate with M_c is inappropriate under such conditions. Although the utility and physical significance of the convective Mach number as originally formulated is limited, various researchers have used it to provide a measure of overall compressibility effects in supersonic mixing flows (e.g. Hall *et al.* 1993).

The current study examines compressible free shear layers under high Mach number conditions which may be experienced in scramjet engines. Previous compressible mixing layer studies have generally focused on mixing at Mach numbers lower than 3; however, the current work examines free shear layer mixing under hypersonic conditions. Primary and secondary streams with nominal Mach numbers of 7 and 3 respectively were used in the present study to generate the free shear layers. The speed of the secondary stream was varied by using gases with differing molecular weights. In this manner, four free shear layer cases with convective Mach numbers ranging from 0 to 1.8 were obtained. A gun tunnel facility with a planar duct and central strut injector were employed to provide hypersonic mixing data in a configuration approaching that of a scramjet engine while retaining some features of previous supersonic mixing layer studies. Thick hypersonic boundary layers were present on the injection strut and represent a significant feature of the flow prior to the formation of the free shear layers. Data on the compressible free shear layers were obtained using schlieren photography and Pitot pressure measurements. The four free shear layer cases ($M_c = 0, 0.5, 1.0, 1.8$) were examined using a parabolized Navier–Stokes code with a k–ϵ turbulence model and included a treatment of the strut boundary layer.

2. Experimental apparatus

2.1. *The gun tunnel*

The University of Oxford gun tunnel is a hypersonic test facility in the Department of Engineering Science. A diagram of the tunnel is shown in figure 1. The operation of the gun tunnel is similar in principle to that of a shock tunnel except that a lightweight piston separates the driver gas from the test gas. Before firing, the piston is placed at the upstream end of the barrel which contains the nitrogen test gas. Behind the piston is a pair of scored aluminium diaphragms which separate the reservoir of high-pressure air (the driver gas) from the piston with a small enclosed volume of gas at an intermediate pressure in the breech. The tunnel is fired by venting the breech which causes the diaphrams to rupture sequentially. The driver gas accelerates the piston

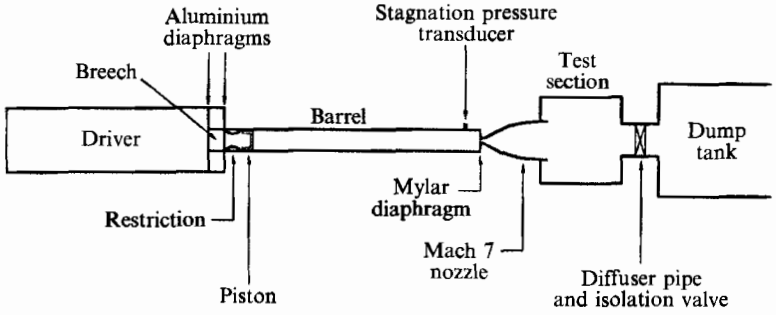

FIGURE 1. Diagram of the University of Oxford gun tunnel facility.

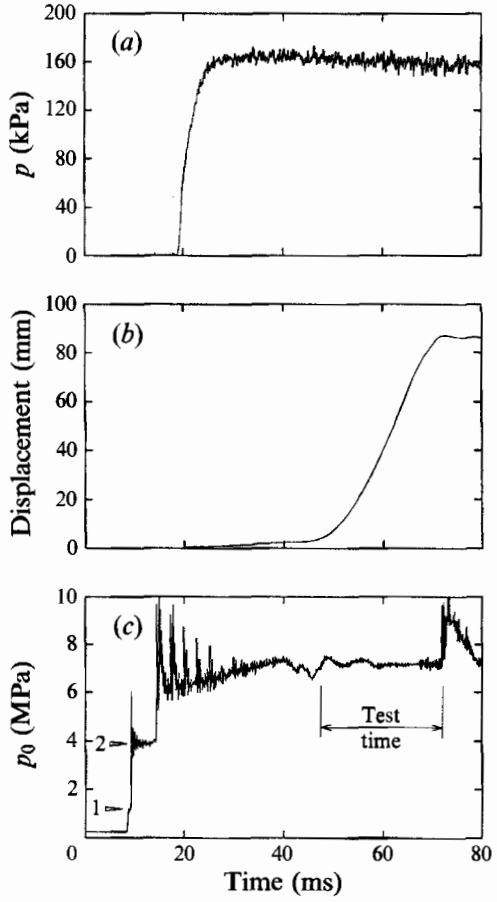

FIGURE 2. Typical signals from various transducers during a test: (*a*) Ludwieg tube pressure, (*b*) Pitot probe displacement, (*c*) gun tunnel stagnation pressure.

which drives a shock wave ahead of it. Upon reaching the end of the barrel, the shock reflects and brings the test gas to rest. When the reflected shock encounters the piston, it reflects again and imparts a further momentum to the test gas. This process continues until the piston is essentially brought to rest and the shock reflections decay into acoustic waves. There follows a period of approximately 30 ms during which the pressure remained essentially constant (to within $\pm 3\%$) – see figure 2. This period was

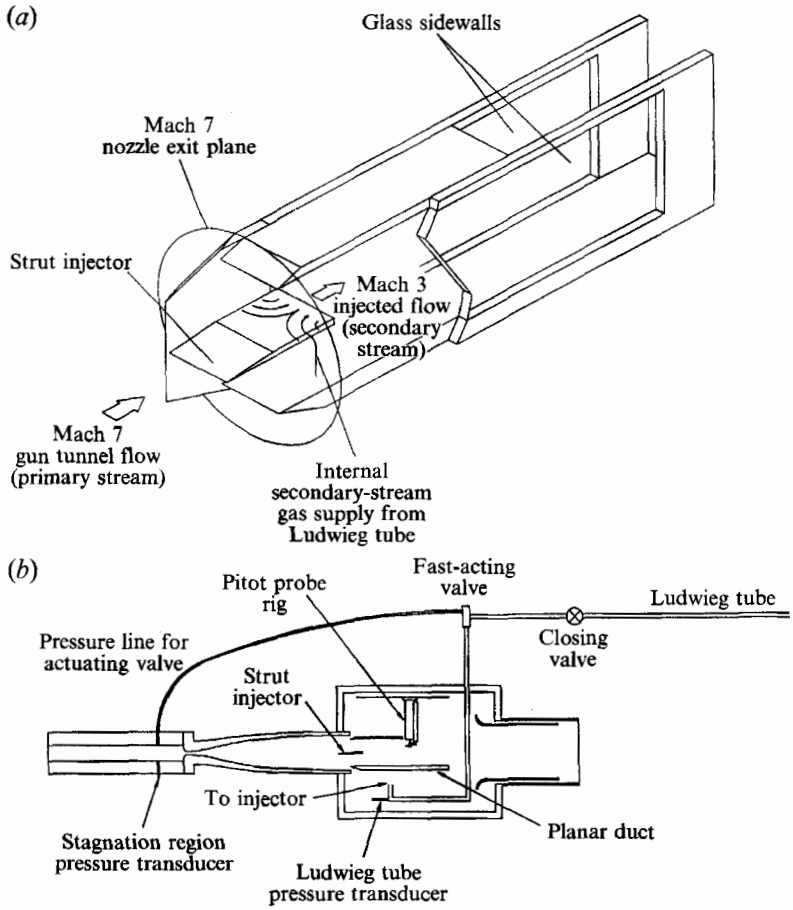

FIGURE 3. Illustration of the planar duct and the configuration of the experimental apparatus: (*a*) three-dimensional sketch of the planar duct; (*b*) sketch of the gun tunnel test section.

regarded as the appropriate test time; the flow measurements reported in the current paper were obtained during this period. A Mach 7 contoured nozzle with an exit diameter of 211 mm accelerated the test gas into the test section after the mylar diaphragm (located between the barrel and nozzle) burst upon shock reflection. Addition details of the present gun tunnel facility may be found in Cain (1991).

2.2. *Experimental rig*

A planar duct, 164 mm high and 80 mm wide, figures 3 and 4, was located centrally in the gun tunnel test section and a secondary stream from the base of a central strut was injected parallel to the primary flow. Steel sidewalls with sharp leading edges held the strut in position. Downstream of the injector, glass sidewalls were installed on the model to allow optical access to the flow field as defined in figure 4. To facilitate the spillage of the waves from the strut leading edge (of importance in later studies), an asymmetric geometry for the leading edge of the strut was employed. The injection strut was 152 mm long in the direction of the main stream and was 7.59 mm thick. The injection strut spanned the planar duct which was 80 mm wide. The leading edge of the injector strut was a 6.6° angle wedge being plane on one side. Ideally, flow underneath the injector would remain undisturbed while the upper flow would be shock

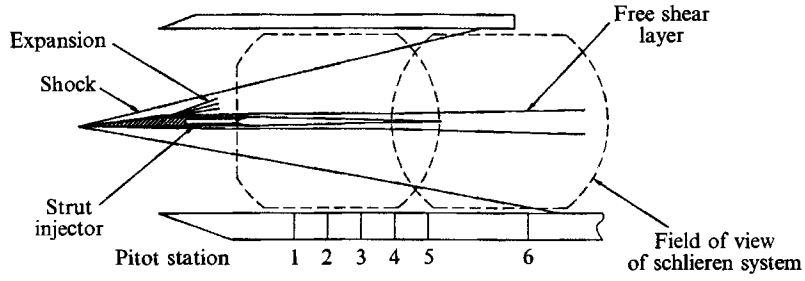

FIGURE 4. Schematic diagram of the planar duct and flow field. Stations 1–6 correspond to Pitot traverses at 40, 70, 100, 130, 160 and 250 mm, respectively downstream from the point of injection.

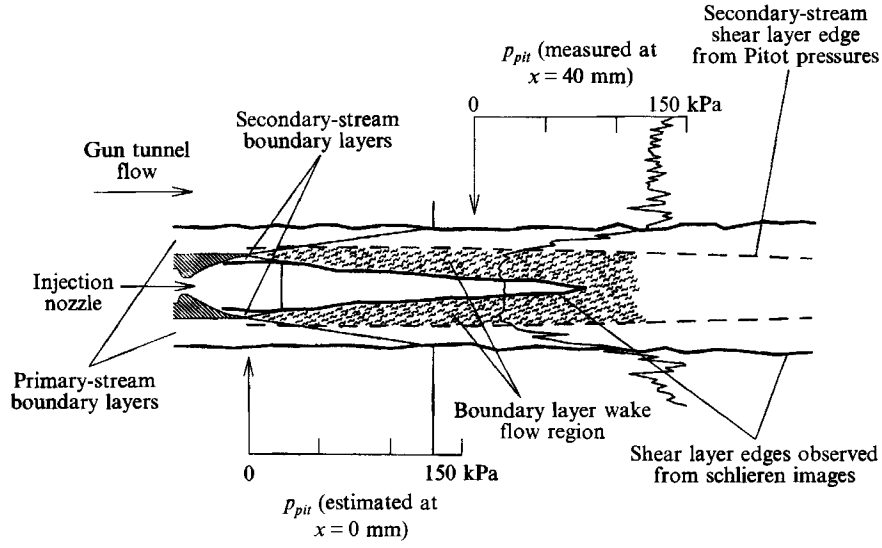

FIGURE 5. Schematic illustration of the formation of the free shear layer from the boundary layers associated with the injection strut and nozzle.

compressed and then re-expanded through an angle of 6.6°, figure 4. In practice, however, boundary layer growth causes added disturbances. For the inviscid case, calculations revealed that the asymmetric geometry would cause a mismatch in static pressures and Mach numbers on either side of the injector trailing edge of less than 0.05% and 2% respectively. This mismatch of conditions was considered to be of little consequence in the present investigation.

The strut injector had a contoured nozzle, designed (using a method of characteristics) to produce a uniform flow with a nominal Mach number of 3, figure 5. The throat of the injector was 1.74 mm high, and the trailing edges were 0.19 mm thick. The Ludwieg tube which supplied the secondary gas to the strut injector, had a 25.4 mm bore and was 25 m long. Internal ducting within the steel sidewalls and central strut delivered the gas to the Mach 3 injection nozzle. A fast acting valve, figure 3, initially isolated the Ludwieg tube from the strut injector. This valve was actuated by the gun tunnel stagnation pressure. The Ludwieg tube was filled with different gas mixtures of hydrogen and nitrogen which gave the four injection conditions presented

Parameter	Primary stream	Secondary stream			
		Case 1	Case 2	Case 3	Case 4
M	7.11	3.24	3.24	3.24	3.24
u (m s^{-1})	1320	1310	1050	854	636
a (m s^{-1})	185	404	324	264	197
T (K)	82.7	93.1	93.1	93.1	93.1
p (kPa)	1.58	1.58	1.58	1.58	1.58
ρ (kg m^{-3})	0.0645	0.0135	0.0211	0.0318	0.0572
ρu (kg m^{-2} s^{-1})	85.0	17.6	22.1	26.9	36.4
ρu^2 (kPa)	112	23.1	23.2	22.9	23.1
μ (N s m^{-2})	5.56×10^{-6}	5.00×10^{-6}	4.99×10^{-6}	4.97×10^{-6}	6.29×10^{-6}
Mass fraction N_2	1.00	0.75	0.87	0.94	1.00
Mass fraction H_2	0.00	0.25	0.13	0.06	0.00
R (J kg^{-1} K^{-1})	297	1254	806	534	297
c_p (J kg^{-1} K^{-1})	1039	4388	2820	1869	1039
Re_u (m^{-1})	15.3×10^6	3.55×10^6	4.43×10^6	5.47×10^6	5.79×10^6
M_c	—	0.02	0.53	1.03	1.79

TABLE 1. Estimated flow parameters

in table 1. Injection of the secondary stream was monitored using a pressure transducer located on the Ludwieg tube ducting within the test section. A typical signal from this transducer for Case 1 is given in figure 2.

2.3. *Instrumentation and data acquisition*

A horizontal knife-edge schlieren system and a Pitot pressure probe were used to investigate the spreading of the free shear layers. The schlieren system employed in the current investigation utilized a horizontal knife edge, and an argon jet light source which produced a spark duration in the order of 0.1 μs. During this time, the maximum flow convection distance is less than 0.2 mm which means that flow features such as shock waves and even two-dimensional large-scale turbulent structures (if present) can be observed reasonably well with this system.

Since there was approximately 30 ms of steady test flow available, it was possible to survey the whole mixing region at a particular streamwise location in a single run. This was achieved using a Pitot probe which was driven across the free shear layer during the test time by a supersonic wing (see figure 2). The maximum transverse velocity of the probe was less than 0.4% of the slowest secondary stream velocity (636 m s^{-1}, Case 4). Thus, the maximum effective yaw angle of the probe (which was less than 0.5°) will have a negligible effect on the pressure measurement. The conclusion that the probe movement had a negligible effect on the measured pressures is supported by the symmetry of the profiles that is observed when the flow is known to be essentially symmetrical (e.g. Morris *et al.* 1995). The pressure signal from the Pitot pressure transducer and the probe displacement (measured with a linear potentiometer, figure 2) were recorded during each traverse.

Signals from the stagnation pressure, injection pressure, Pitot pressure, probe displacement, test section pressure and schlieren spark timing were multiplexed into a single Hewlett Packard 12 bit data logger and were subsequently processed using personal computers. Each signal was sampled at approximately 13 kHz, except for the Pitot pressure which was sampled at approximately 26 kHz.

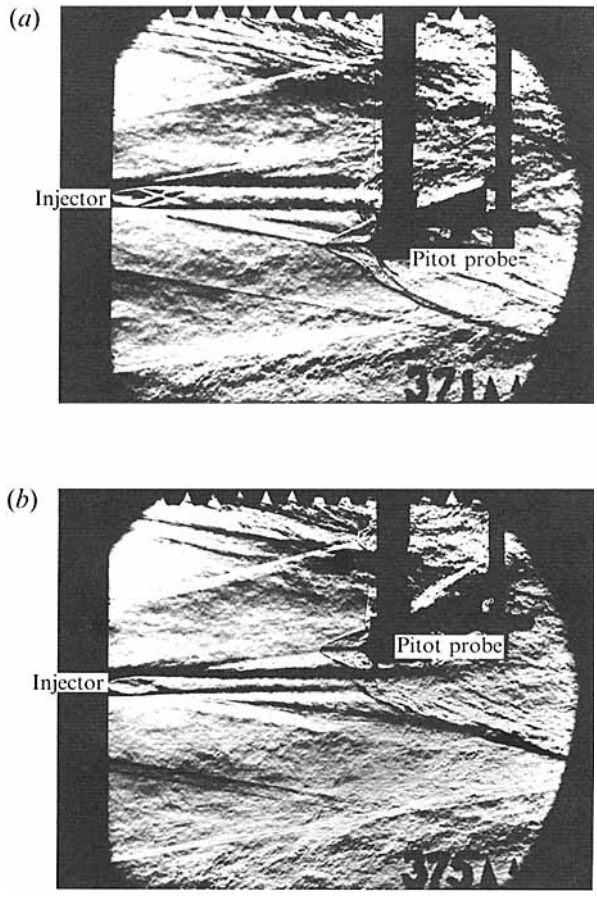

FIGURE 6. Schlieren images for (*a*) under- and (*b*) over-expanded nitrogen injection. Each division at the top of the photographs = 1 cm. Ludwieg tube filled to (*a*) 1.4 and (*b*) 0.64 times the matched injection pressure condition.

2.4. *Primary and secondary stream conditions*

The primary-stream conditions generated by the gun tunnel are shown in table 1. The calculation of these conditions was based on the measured stagnation pressure (such as given in figure 2), and the Pitot pressure measured at the exit of the Mach 7 nozzle. For the calculation of the stagnation temperature, it was assumed that during the gun tunnel compression process, the magnitude of each shock velocity jump was the same, and that no further entropy rise was produced after the action of the fourth shock. The shock velocity jump can be determined from the pressures measured behind the first and second shocks (marked 1 and 2 in figure 2). The stagnation temperature of the test gas was obtained using the stagnation pressure measured during the test time and the entropy rise calculated for the shock compression process. Preliminary fast-response total temperature measurements have confirmed this approach. The gun tunnel nozzel exit conditions (such as the Mach number, temperature, and pressure) were found from the measured exit Pitot pressure and the stagnation conditions determined above.

The Mach number of the secondary flow was determined through measurements of Pitot pressure at the injector nozzle exit and total pressure at the throat of the injector. These measurements were made using a probe with a 1 mm diameter tube at the mid-span of the injector. Since the change in throat area caused by the presence of the probe

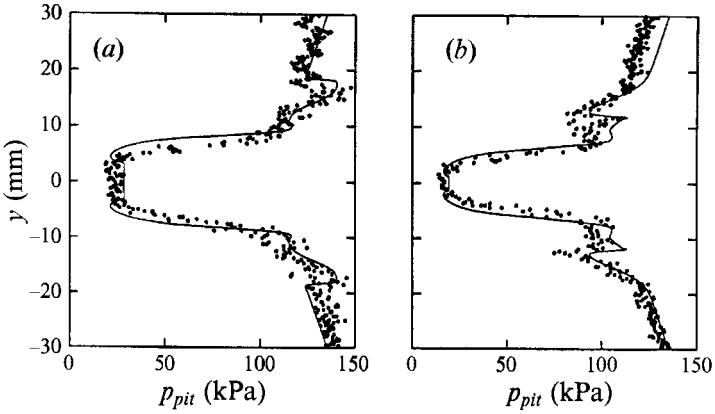

FIGURE 7. Pitot pressure results at Station 2 for (*a*) under- and (*b*) over-expanded injection cases shown in figure 6: ——, PNS code; ●, experiment.

was less than 1%, the calibration technique was considered to be reasonable. Secondary-stream injection conditions (also presented in table 1) were calculated using this Mach number and assuming a measured Ludwieg tube total temperature of 288 K.

Pressure matching of two streams was achieved through repeated Pitot pressure measurements and schlieren images taken at different Ludwieg tube filling pressures using nitrogen. When visualization of the flow structure indicated matched pressures, and no waves from the injection process were detected using the Pitot probe at 70 mm downstream from the base of the strut injector, the pressures of the two flows were assumed to be matched. Examples of under- and over-expanded injection conditions for Ludwieg tube filling pressures of 1.4 and 0.64 times that of the match pressure condition are given in figures 6 and 7. The different total thicknesses of the free shear layer, and the wave patterns generated at the lip of the injector as detected with the Pitot probe should be noted.

3. Results

3.1. *Schlieren flow visualization*

The general features of the schlieren images for each mixing case, such as the wave patterns, boundary layers, and free shear layers, appeared to be very similar. A composite image for Case 4 is presented in figure 8. Shock waves originating from the leading edge of the asymmetrical strut are clearly visible on both sides of the injector in figure 8. The shock wave on the lower strut surface can be attributed to the rapid growth of a hypersonic boundary layer – a hypersonic viscous interaction effect. The schlieren images also record the propagation of disturbances originating at the trailing edge of the injector. In the under- and over-expanded injection conditions, these waves are clearly related to the necessary flow readjustment to the pressure mismatch. At the matched pressure conditions, such disturbances are weak and may be related to the finite thickness of the injector trailing edges. In the matched pressure case there appears to be a slight transmission of these disturbances into the primary stream (see figure 9, Station 1, at $y = -10$ mm); however, it is confirmed that these disturbances are weak since no such waves were detected with the Pitot probe by Station 2.

Within the gun tunnel test section, the flow static pressure inside the model was lower than the background pressure, owing to the slight diffuser blockage caused by the model. Hence, a converging conical shock wave formed at the edge of the Mach 7

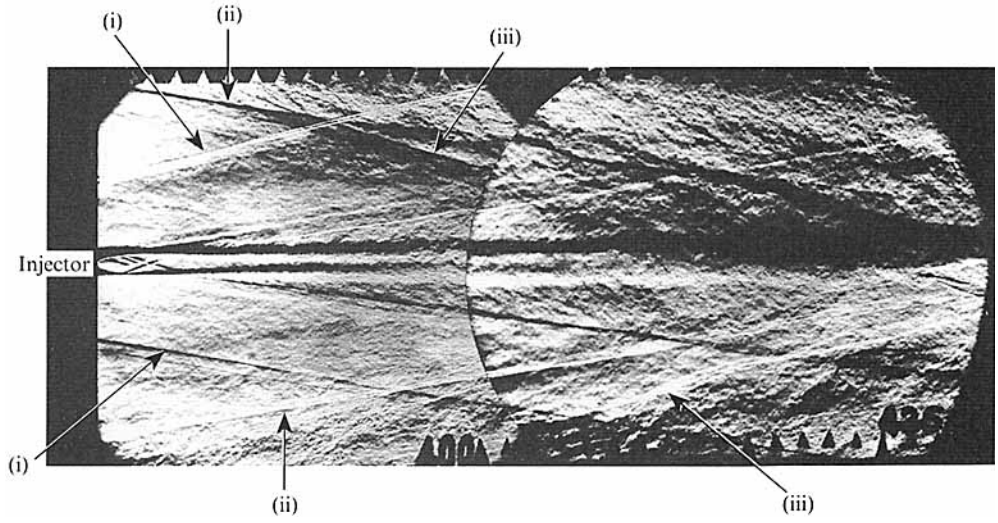

FIGURE 8. Composite schlieren image from the Case 4 free shear layer. Each division at the top of the photographs = 1 cm. (i) Strut injector shocks; (ii) upper and lower cowl shocks; (iii) test diamond exit shocks.

nozzle. This shock, which can be seen in the schlieren images, is outside the planar duct, and did not affect the integrity of the experiments. It did, however, provide a confusing addition to the schlieren images, and varied in strength depending on the test section static pressure. For example, in the first photograph of the composite image in figure 8, the Pitot probe was located at Station 6 and blocked the passage of the flow into the diffuser, causing the test section pressure to rise, producing a relatively strong test diamond shock wave. In the second photograph of this composite image, the nozzle shock wave is considerably weaker because the Pitot probe was removed which allowed the test section pressure to be maintained at a lower level.

Significant hypersonic boundary layers developed on the strut injector, and at the trailing edge; they each appear to be approximately 3.2 mm thick. Boundary layer regions are also visible in the Mach 3 injector nozzle. From the schlieren images, these boundary layers are estimated to be 0.7 mm thick at the trailing edge of the injector.

The visual thickness of the shear layer determined using schlieren can be a very subjective measurement, and may depend to some extent on the sensitivity of the system. Nevertheless, it is clearly evident that there is very little growth of the free shear layer into the primary stream. In comparison, the shear layers from both splitter plates appear to grow quite rapidly into the secondary stream, and at approximately 60 mm downstream of the injector, the edges of the two layers appear to merge at the centreline of the jet (see figure 8). The turbulent nature of the free shear layers is clearly apparent from the irregularity of the visible edges of the layers. However, no large-scale two-dimensional structures were observed in any of the images, nor was there evidence of any travelling shock waves associated with the turbulent structures.

3.2. *Pitot pressure traverses*

Distributions of Pitot pressure across the free shear layer at the six stations in figure 4, which correspond to $x = 40$, 70, 100, 130, 160 and 250 mm, are presented in figure 9 for each of the four conditions. The origin for the x- and y-coordinates is taken as the trailing edge and the centreline of the injector respectively. Slight differences between the profiles can be discerned in some cases. For example, at locations downstream of

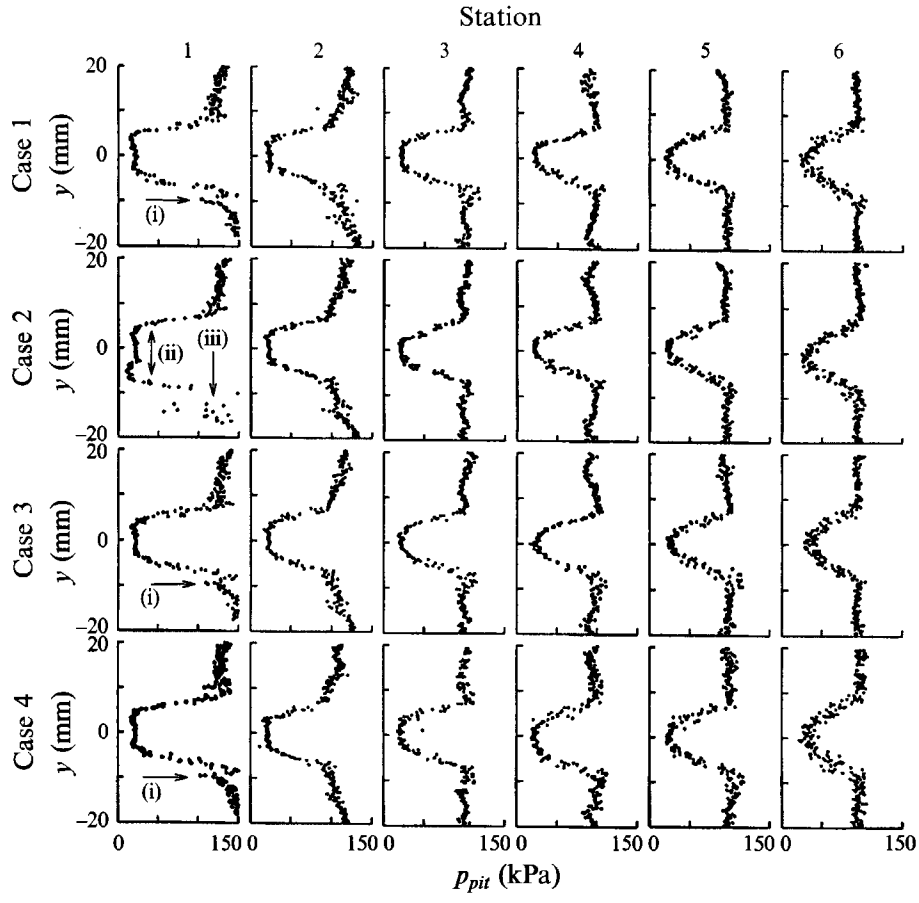

FIGURE 9. Matrix of Pitot pressure traverses. (i) Weak wave disturbance in the primary free stream; (ii) increased size of low-pressure region associated with choking; (iii) increased irregularity of Pitot pressure associated with choking.

Station 3, Case 4 produced fuller Pitot profiles than Case 2. However, considering the wide variation of the injection conditions (see table 1), the profiles for all cases are remarkably similar.

To determine the spreading of the free shear layers from the Pitot results, a definition of the location of the shear layer edge, or shear layer thickness is necessary. Following Papamoschou & Roshko (1988), the 5% Pitot pressure shear layer thickness as defined in figure 10 will be adopted for the current analysis. Thicknesses t_1 and t_2 were measured from the Pitot profiles after a curve was fitted to the data. The half-thicknesses, $t_1/2$ and $t_2/2$, are plotted in figure 11, along with the estimated uncertainties in determining these values. Pitot pressures significantly higher than expected in the undisturbed free stream (103 kPa at Mach 7) were measured in the primary stream at Stations 1 and 2 (see figure 9). These deviations can be attributed to the growth of the hypersonic boundary layers on the injector strut and sidewalls of the duct.

Even under conditions of matched pressure, a wave disturbance on the lower side of the injector at Station 1 was observed in Cases 1, 3 and 4 around $y = -10$ mm (feature (i) in figure 9). The fact that this disturbance was not observed on both sides of the strut may be related to the asymmetric leading-edge geometry of the injector. Total

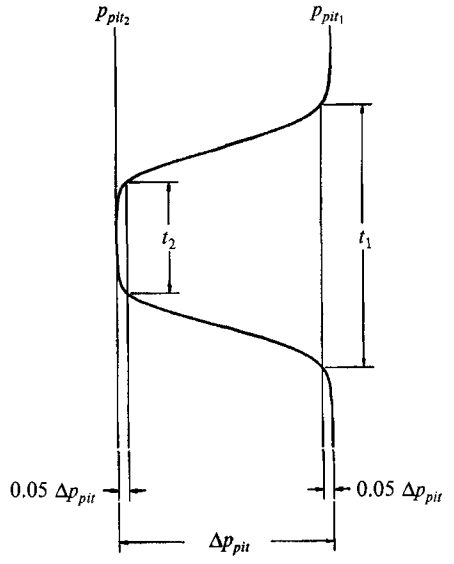

FIGURE 10. Definition of shear region thicknesses used in the current study.

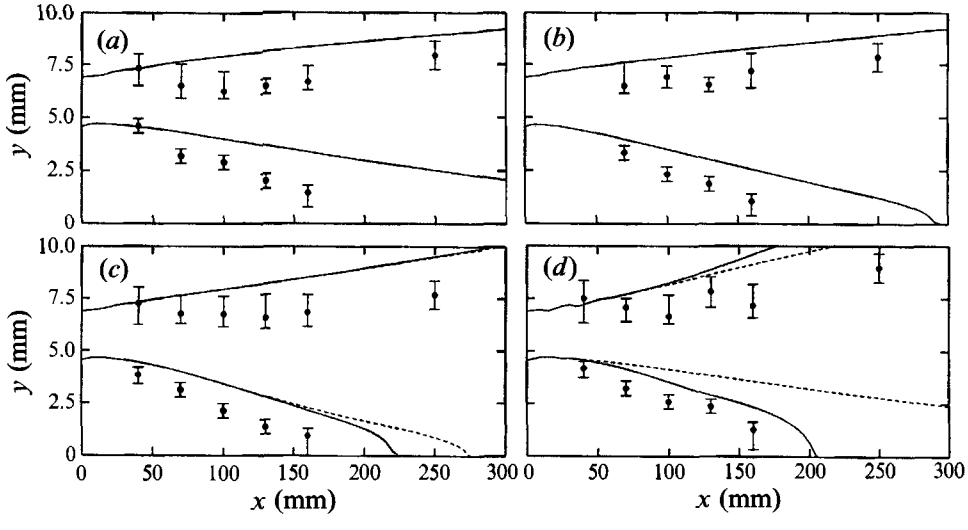

FIGURE 11. Extent of free shear layers from Pitot measurements. Solid lines are results from PNS code using k–ϵ model, dashed lines are results using k–ϵ model with the compressibility correction. (*a*) Case 1, (*b*) Case 2, (*c*) Case 3, (*d*) Case 4.

elimination of all waves arising from the injection process in the current configuration seems, for practical purposes, impossible because of disturbances arising due to finite splitter-plate thicknesses, and the possibility of three-dimensional effects. Apart from this relatively minor effect, the distribution of Pitot pressure in the vicinity of the free shear layers was essentially symmetrical about the centreline of the jet. No difference in the development of the upper and lower free shear layers was detected with either the schlieren system or Pitot pressure measurements.

At Station 1, the Pitot probe support and drive caused a substantial flow blockage effect, particularly as it approached the extent of its travel. If choking occurred, the test

section pressure rose sharply, and the Pitot pressure began to fluctuate wildly. A schlieren image of a Pitot traverse at $x = 32$ mm, taken when the probe was at $y = -28$ mm, shows subsonic flow around the probe for $y < 0$ (as evidenced by the unusual lack of shock waves) and the separation of the lower-strut boundary layer (Buttsworth 1994). Separation of the lower-strut boundary layer and the early onset of choking is also apparent in the Pitot pressure profile of Case 2 at Station 1 (figure 9) as evidenced by the increased size of the low-pressure region (feature (ii) in figure 9) which extends from approximately $y = -8$ to 4 mm compared with $y = -4$ to 4 mm in the other three cases at Station 1, and the relative irregularity of the Pitot pressure in the region $y < -5$ mm (feature (iii) in figure 9). Except at locations upstream of Station 1, chocking was not a problem and, typically, the flow behaved in a regular manner with the shock generated by the Pitot probe rig remaining close to the probe throughout the majority of the traverse as recorded by the schlieren images in figure 6.

4. Discussion

4.1. *Initial conditions*

The initial boundary layers and the inviscid flow field can both influence the development of mixing layers, so it is important to address these aspects prior to discussing the mixing layers themselves. Stollery (1967) reported results from flat-plate boundary layer transition experiments using another gun tunnel facility at conditions similar to those of the current investigation. Using a contoured Mach 8 nozzle, and a unit Reynolds number of 16.6×10^6 m^{-1} (cf. Mach 7 and $Re_u = 15.3 \times 10^6$ m^{-1} in the present study), transition began at a Reynolds number of 2.52×10^6, and was not completed until 4.45×10^6 (cf. $Re = 2.33 \times 10^6$ at the trailing edge of the strut injector). Applying the van Driest boundary layer solution (White 1991) at these conditions, the thickness of a compressible laminar flat-plate boundary layer was calculated to be 1.4 mm. However, from the schlieren measurements, the observed boundary layer thickness is over twice this value. These results suggest that the high-speed boundary layers at the trailing edge of the strut are at least transitional, but may not yet be fully turbulent.

Calculations of the injector strut flow field were performed using a two-dimensional steady parabolized Navier–Stokes (PNS) code (Brescianini 1992*a*) which has already been validated and successfully applied to the study of various supersonic mixing and combustion problems (Brescianini 1992*a*, *b*; Brescianini & Morgan 1992, 1993; Bakos & Morgan 1992). At a station 28 mm downstream of the injector trailing edge, the Pitot traverse, figure 12, clearly shows the free stream ($y > 39$ mm, region (i) in figure 12), the upper shock from the strut injector ($y = 39$ mm, location (ii) in figure 12), and the corner expansion ($39 > y > 25$ mm, region (iii) in figure 12). For the PNS calculations, the strut was assumed to continue downstream to this station. From figure 12, the PNS calculation with a turbulent boundary layer predicts a shock location and strength, and a post-expansion Pitot pressure that are in better agreement with the experimental results than the laminar boundary layer calculation. However, the turbulent calculation predicts a boundary layer thickness of 5.91 mm on the upper side of the strut, which is significantly larger than the visual thickness. An important limitation of these PNS calculations is that the turbulent boundary layer necessarily began at the strut leading edge since no model for transition was incorporated into the code. Nevertheless, the turbulent prediction clearly demonstrates that the presence of boundary layers on the injector strut can increase the high primary stream Pitot pressures measured at Stations 1 and 2.

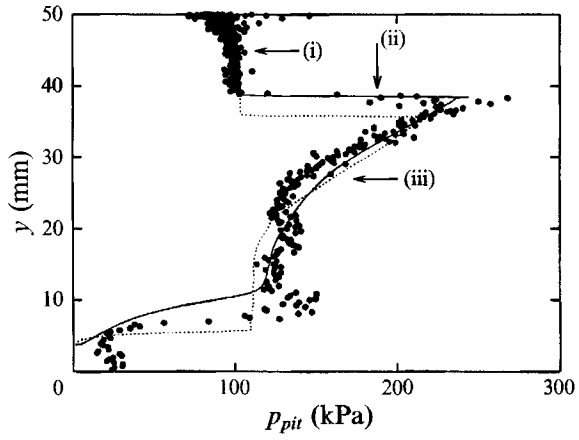

FIGURE 12. Pitot pressure at a station 28 mm downstream of the injector. PNS calculations assuming either a laminar (.....) or turbulent (——) boundary layer, and experiment (●). (i) Free stream region; (ii) upper shock from strut injector; (iii) expansion fan region.

Case	$\frac{1}{2}(dt_1/dx)$	$\frac{1}{2}(dt_2/dx)$
1	0.004	−0.025
2	0.007	−0.024
3	0.003	−0.025
4	0.008	−0.022

TABLE 2. Spreading rates of the shear layer edges from the Pitot pressures

4.2. *Modelling the initial conditions*

In all of the PNS free shear layer calculations, the primary- and secondary-stream boundary layers were set to a thickness of 3.23 mm and 0.92 mm respectively. The secondary-stream boundary layer was set at approximately 0.2 mm larger than the measured schlieren thickness so as to include the finite thickness of the trailing edge of the injector strut. Turbulent boundary layers with a 1/7 power-law velocity distribution were assumed for both the primary- and secondary-stream boundary layers. Since the free shear layers that formed at the trailing edges of the strut injector appeared to be essentially symmetric about the centreline of the strut injector, only half of the flow field was modelled.

For the PNS calculations of the free shear layers, attempts were made to model the higher primary-stream Pitot pressures measured upstream of Station 2. Primary-stream conditions at the injector trailing edge were set empirically so as to match the observed Pitot pressure distribution downstream of the injector in the matched pressure case. With this method, a degree of success was achieved in the modelling of the under- and over-expanded injection conditions, figure 7. However, a number of deficiencies in this method arose because in essence, the code was two-dimensional.

4.3. *Free shear layer growth*

In the study of supersonic mixing, attention is often focused on achieving fully developed mixing layers (Clemens & Mungal 1992) owing to their fundamental nature. None of the four current mixing layer cases reached a fully developed state according to the definition of Goebel & Dutton (1991) before merging on the centreline of the jet

occurred. However, studies of mixing layers prior to a fully developed state have also been conducted (e.g. Kwok *et al.* 1991) and are important because of the low mixing rates and large boundary layer regions anticipated in full-scale supersonic combustors.

In all of the four cases of the present study, the secondary stream (the jet) was injected at a speed lower than or approximately equal to that of the primary stream. For scramjet-powered flight above Mach numbers of approximately 12, the fuel will be injected at speeds lower than the air stream velocity, and at flight Mach numbers approximately equal to 12 the fuel and air streams will move at approximately the same velocity (Anderson, Kumar & Erdos 1990). Therefore, each of the free shear layer cases presently studied, including the matched velocity case, is relevant to the development of scramjet propulsion at approximately Mach 12 or faster.

Using conditions given in table 1 as the initial conditions, the PNS code was run for each of the four free shear layers. The primary stream at the injector trailing edge was assumed uniform, and the initial normalized length scale (= initial length scale/shear region width) for the k–ϵ model was set to 0.03. In figure 11, half of the predicted 5% Pitot pressure thickness (as defined in figure 10) has been presented along with the experimental results for comparison. Attempts were made to 'tune' the free shear layer model to the experimental results by adjusting the initial normalized length scale. However, a good simultaneous agreement of the primary- and secondary-stream spreading rates could not be achieved in any of the cases. Although a degree of asymmetry is predicted by the k–ϵ model, its extent does not match the experimental results. When considering this disparity, it is worth recalling that in the free shear layer modelling, fully developed turbulent boundary layers were necessarily assumed (as the PNS code does not model transition) on both the primary and secondary-stream sides of the injection nozzle, whereas experimentally this was probably not the case.

Brescianini (1992*b*) recently proposed a compressibility correction to the k–ϵ model which improved the prediction of the spreading rates of developed supersonic mixing layers. When this correction was used, it made little apparent difference in the two lower-compressibility shear layers, Cases 1 and 2. However, in Cases 3 and 4, the predicted spread of the shear layer into primary and secondary streams became more symmetrical, in contrast to the experimentally observed asymmetrical spreading. It appears that Brescianini's compressibility correction is not well suited to the prediction of the current undeveloped, high Mach number free shear layers.

Although in the current study the predicted shear layer spreading rate varied from case to case, the experimental Pitot results indicate that, for all of the cases, the secondary stream growth rate was about 0.024 (see table 2), and the primary-stream growth rate was essentially 0 over the first five stations. The results given in table 2 (obtained from a linear regression for the data in figure 11) do not fully reflect the severe asymmetry of the shear layer spreading up to Station 5 ($x = 160$ mm), since there appears to be an acceleration in the spreading of the primary-stream edge between Stations 5 and 6 ($x = 160$ and 250 mm). A severe asymmetry in the spreading rates of compressible mixing layers was likewise observed by Erdos *et al.* (1992). In a hypervelocity mixing layer configuration they observed virtually no spreading into the primary stream until the edge of the layer reached the secondary-stream wall, at which stage the primary-stream shear layer growth rate noticeably increased. A similar effect is apparent in the present experimental results which indicate very little primary growth until $x = 250$ mm (Station 6), by which stage the two mixing layers have reached the jet centreline. Following the suggestion of Erdos *et al.* (1992), this increase in primary-stream growth rate might stem from a change in the character of the turbulence upon reaching a boundary, which in the present study is a plane of symmetry.

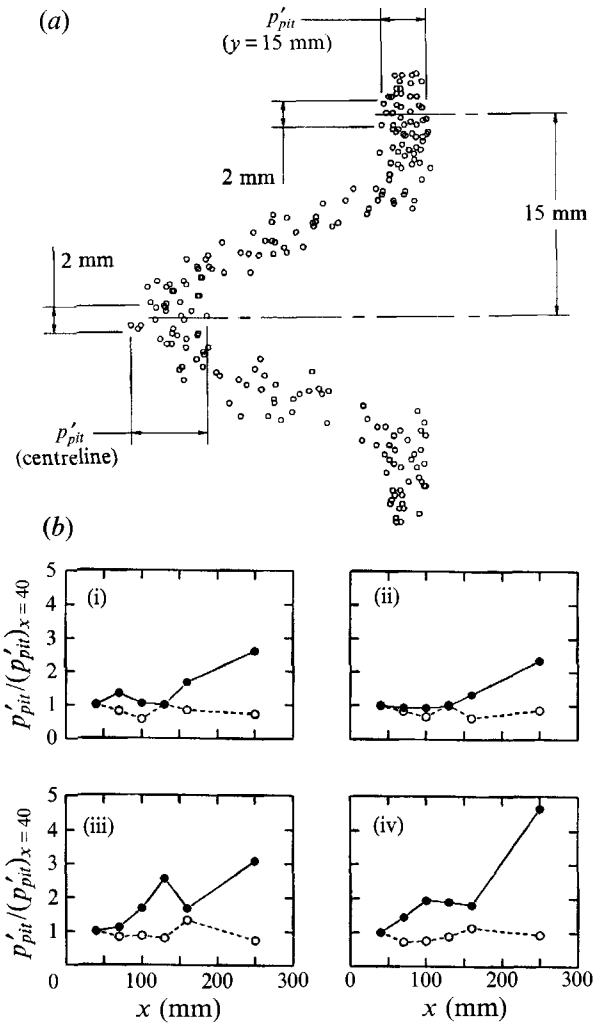

FIGURE 13. Pitot pressure fluctuations measured on the centreline of the injected flow (●) and in the primary free stream at $y = 15$ mm (○). (*a*) Illustration of the measurement of pressure fluctuations from the Pitot traverse. (*b*) Results for the four mixing cases: (i) Case 1, (ii) Case 2, (iii) Case 3, (iv) Case 4.

Figure 13(*a*) is schematic illustration of the Pitot pressure measurements from a particular traverse. From such measurements (i.e. the Pitot results presented in figure 9), the peak-to-peak fluctuations in the Pitot pressure (p'_{pit}) measured across a transverse distance of 2 mm on the centreline of the injected flow and at $y = 15$ mm (see figure 13*a*) were obtained. The values of p'_{pit} obtained on the centreline and at $y = 15$ mm for the six Pitot stations ($x = 40$, 70, 100, 130, 160 and 250 mm) were normalized by the respective fluctuations obtained at Station 1 ($x = 40$ mm); these normalized results are presented in figure 13(*b*). Pitot pressure fluctuations have previously been used to obtain turbulence data (e.g. Shau & Dolling 1992). However, in the present work, the Pitot pressure fluctuations are used simply as an indication of the relative level of turbulent activity.

As expected, the level of the measured primary-stream Pitot pressure fluctuations remained essentially constant (at approximately ±5% of the primary-stream Pitot

pressure level) across the six measurement stations. However, at the centre of the secondary stream, a significant increase in fluctuation level occurred between Stations 5 and 6 ($x = 160$ and 250 mm). (The initial secondary-stream fluctuations correspond to approximately $\pm 3\%$ of the secondary-stream Pitot pressure level.) The increase in secondary-stream fluctuation level supports the hypothesis that the increase in spreading rates between Stations 5 and 6 can be related to a change in the turbulence properties that occurs when the free shear layers meet on the centreline of the secondary stream. It is of interest to note that the turbulence properties at the centre of the secondary stream do not change immediately with the merging of the mixing layers at approximately $x = 60$ mm as indicated by the schlieren images.

Preferential entrainment of the secondary stream is not unexpected because the momentum of the primary stream is approximately 5 times larger than the secondary stream momentum (see table 1). The shear regions on either side of any streamline see an equal and opposite shear stress, which, assuming a constant pressure and the absence of any external forces, means that

$$\rho_1 u_1^2 \frac{\mathrm{d}\theta_1}{\mathrm{d}x} = -\rho_2 u_2^2 \frac{\mathrm{d}\theta_2}{\mathrm{d}x}, \tag{2}$$

where θ_1 and θ_2 are the momentum thicknesses of the regions to either side of the splitter-plate streamline, referenced to their respective free streams. Therefore, in the present cases, considerable asymmetry may be expected since the secondary-stream momentum thickness growth rate will be approximately 5 times that of the primary stream. However, it should be noted that the profiles of the present layers were not self-similar, meaning that the momentum thickness growth rates may not translate directly into physical shear layer growth rates. That is, the momentum thickness of each region may change due to internal redistribution of the velocity profile in the layer, rather than by transverse spreading.

The resemblance of each mixing case may be related to the dominant role that the primary-stream boundary layers had in the development of mixing. Using a boundary layer thickness of 3.2 mm, a 1/7th power-law velocity profile, and a temperature distribution according to the Crocco–Busemann relationship, it was estimated that the combined momentum deficit of the gas within the primary-stream boundary layers on the injector strut represented 60% of the momentum deficit of the secondary-stream gas (relative to the primary stream). Thus, the combined momentum deficit of the primary-stream boundary layers was comparable to that of the secondary stream in each mixing case. Therefore, it may be concluded that the primary-stream boundary layers on the injector strut will play an equally significant role in the development of the free shear layers in each mixing case. (The momentum of the secondary-stream boundary layers was estimated to be less than 10% of that of the primary stream. Thus, the secondary-stream boundary layers are likely to have a relatively small influence on the free shear layer development.)

From the schlieren images, very little growth of the layers into the primary stream was observed, which accords well with the experimental Pitot pressure results. However, for the growth into the secondary stream, the schlieren images indicate that the two mixing layers merged on the jet centreline at around $x = 60$ mm whereas the Pitot results indicate a value of about 200 mm (see figure 11) around three times larger. The apparent discrepancy is due to the definition of the Pitot pressure thickness (figure 10) which actually locates the initial secondary-stream Pitot pressure edge in the lower part of the primary-stream boundary layer because of the boundary layer wake flow region near the trailing edge of the injector (see figure 5). This wake region contributes

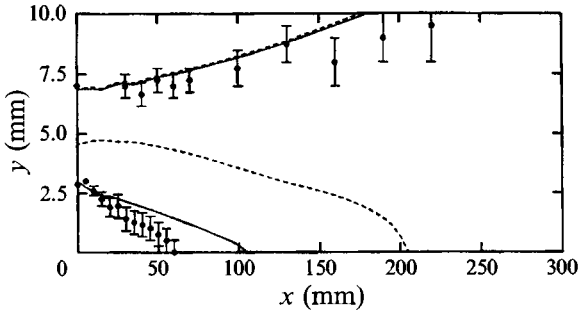

FIGURE 14. Schlieren data and PNS calculations for Case 4 showing a comparison of shear layer edge definitions: ——, density edge; – – –, Pitot edge; ●, Schlieren data.

to the visible shear layer thickness but remains undetected by the Pitot pressure measurements, except at Station 1. That is, from the Pitot pressure measurements at Stations 2 to 6, the boundary layer wake flow region appears to be part of the secondary free stream.

As a demonstration of this effect, the primary- and secondary-stream mixing layer edges, defined by the locations at which the density within the layer reached a value 5% lower than the primary and secondary free streams (respectively), were plotted for the PNS calculation of Case 4 along with the Pitot shear layer edges in figure 14. From these results it is clear that the actual secondary-stream mixing layer edge is not accurately determined by the Pitot results, while the primary-stream free shear layer edge is correctly located by the Pitot pressure. Based on the schlieren results, it appears that the spreading of the mixing layers is even more asymmetric than indicated by the Pitot data. For example, in Case 4, according to the Pitot data in table 2, the mixing layer spreads into the secondary stream at a rate of 0.022 whereas, according to the schlieren data presented in figure 14, the spreading rate was 0.048, which is over twice as large.

5. Conclusions

Experimental investigations into the spreading of compressible free shear layers have been conducted using a planar duct with central strut injection in a gun tunnel facility. The Mach numbers generated in the primary and secondary streams were 7.1 and 3.2 respectively, and four different shear layer conditions ranging in convective Mach number from 0 to 1.8 were attained by altering the molecular weight of the secondary stream. The primary-stream flow velocity was approximately 1300 m s^{-1}, and the lowest-speed secondary stream had a velocity of 640 m s^{-1}. Schlieren images and Pitot pressure measurements at 6 stations downstream of the injector were taken in each free shear layer case.

Hypersonic boundary layers developed on the strut injector caused an increase in the primary-stream Pitot pressure measured at locations close to the injector. Only small differences in the Pitot profiles of the four cases could be discerned, and the spreading rates determined from the Pitot measurements did not vary dramatically from that experienced when both streams moved at approximately the same velocity. This result suggests that the initial boundary layer played an important role in the development of the free shear layer in each case. For the free shear layers studied in the present experiments, the spreading rate appears to be independent of the convective Mach number.

Considerable asymmetry of the free shear layers was observed in both the schlieren and Pitot pressure results. From the Pitot results, each of the four shear layers spread into the secondary stream at a rate of approximately 0.024, and virtually no spreading into the primary stream was observed until the secondary stream was fully entrained. The schlieren images indicate a secondary-stream shear layer growth rate twice as large as was evident in the Pitot results owing to a boundary layer wake region effect. Pitot pressure fluctuations indicated that a significant increase in turbulent activity at the centreline of the jet occurred between the last two Pitot pressure measurement stations. This location is approximately coincident with the primary-stream shear layer growth rate increase which occurs well after the free shear layers reach the jet centreline according to the schlieren visualization.

The experimentally observed degree of asymmetry in the free shear layer spreading rate could not be predicted using a PNS calculation with a k–ϵ model in any of the cases. However, the assumption of a fully turbulent high-speed boundary layer may be a significant factor contributing to the differences between the experimental and predicted results since experimentally the high-speed boundary layer appeared to be in transition. A compressibility correction to the k–ϵ model, which improved the predicted spreading rates of developed supersonic mixing layers, was less successful than the usual model in predicting the asymmetric spreading of the current free shear layers. The fundamental nature and relevance of the present data to scramjet mixing and combustion systems warrants further modelling and experimentation in similar configurations.

The first author gratefully acknowledges the financial support of The British Council through the Post-Graduate Research Bursary scheme. Financial support of the gun tunnel facility was granted by DRA Farnborough. The authors wish to thank Dr Noel Morris and Dr Terry Cain for their valuable contributions to this work. The assistance of the Osney Laboratory technical staff was greatly appreciated. Dr Craig Brescianini is also sincerely thanked for making his PNS code available and friendly.

REFERENCES

ANDERSON, G., KUMAR, A. & ERDOS, J. 1990 Progress in hypersonic combustion technology with computation and experiment. *AIAA Paper* 90-5254.

BAKOS, R. J. & MORGAN, R. G. 1992 Axisymmetric scramjet thrust production. *11th Australasian Fluid Mechanics Conference*, pp. 295–298.

BIRCH, S. F. & EGGERS, J. E. 1973 A critical review of the experimental data for developed free turbulent shear layers. In *Free Turbulent Shear Flows*, vol. 1, NASA SP-321, pp. 11–40.

BLUMEN, W., DRAZIN, D. G. & BILLINGS, D. F. 1975 Shear layer instability of an inviscid compressible fluid. *Part* 2. *J. Fluid Mech.* **71**, 305–316.

BOGDANOFF, D. 1983 Compressibility effects in turbulent shear layers. *AIAA J.* **21**, 926–927.

BRESCIANINI, C. P. 1992*a* An investigation of the wall-injected scramjet. PhD Thesis, Department of Mechanical Engineering, University of Queensland.

BRESCIANINI, C. P. 1992*b* Modified k–ϵ model for compressible free shear flows *AIAA J.* **30**, 2161–2163.

BRESCIANINI, C. P. & MORGAN, R. G. 1992 An investigation of a wall-injected scramjet using a shock tunnel. *AIAA Paper* 92-3965.

BRESCIANINI, C. P. & MORGAN, R. G. 1993 Numerical modeling of wall-injected scramjet experiments. *J. Propulsion Power* **9**, 169–175.

BROWN, G. L. & ROSHKO, A. 1974 On density effects and large structure in turbulent mixing layers. *J. Fluid Mech.* **64**, 775–816.

BUTTSWORTH, D. R. 1994 Shock induced mixing and combustion in scramjets. PhD Thesis, Department of Mechanical Engineering, The University of Queensland.

CAIN, T. M. 1991 An experimental study of underexpanded jets. D.Phil. thesis, Department of Engineering Science, University of Oxford.

CHINZEI, N., MASUYA, G., KOMURO, T., MURAKAMI, A. & KUDOU, K. 1986 Spreading of two-stream supersonic turbulent mixing layers. *Phys. Fluids* **29**, 1345–1347.

CLEMENS, N. T. & MUNGAL, M. G. 1992 Two- and three-dimensional effects in the supersonic mixing layer. *AIAA J.* **30**, 973–981.

CLEMENS, N. T. & MUNGAL, M. G. 1995 Large-scale structure and entrainment in the supersonic mixing layer. *J. Fluid Mech.* **284**, 171–216.

DIMOTAKIS, P. E. 1991 Turbulent free shear layer mixing and combustion. In *Progress in Astronautics and Aeronautics*, Vol. 137: *High-Speed Flight Propulsion Systems* (ed. S. N. B. Murthy & E. T. Curran) pp. 265–340. AIAA.

DRUMMOND, J. P., CARPENTER, M. H. & RIGGINS, D. W. 1991 Mixing and mixing enhancement in supersonic reacting flowfields. In *Progress in Astronautics and Aeronautics*, Vol. 137: *High-Speed Flight Propulsion Systems* (ed. S. N. B. Murthy & E. T. Curran) pp. 383–455. AIAA.

ELLIOTT, G. S. & SAMIMY, M. 1990 Compressibility effects in free shear layers. *Phys. Fluids* A **2**, 1231–1240.

ELLIOTT, G. S., SAMIMY, M. & ARNETTE, S. A. 1992 Study of compressible mixing layers using filtered Rayleigh scattering based visualizations. *AIAA J.* **30**, 2567–2569.

ERDOS, J., TAMANGO, J., BAKOS, R. & TRUCCO, R. 1992 Experiments on shear layer mixing at hypervelocity conditions. *AIAA Paper* 92-0628.

GOEBEL, S. G. & DUTTON, J. C. 1991 Experimental study of compressible turbulent mixing layers. *AIAA J.* **29**, 538–546.

GROPENGIESSER, H. 1970 Study of the stability of boundary layers in compressible fluids. *NASA TT-F*-12.

HALL, J. L., DIMOTAKIS, P. E. & ROSEMAN, H. 1993 Experiments in nonreacting compressible shear layers, *AIAA J.* **31**, 2247–2254.

KWOK, K. T., ANDREW, P. L., NG, W. F. & SCHETZ, J. A. 1991 Experimental investigation of a supersonic shear layer with slot injection of helium, *AIAA J.* **29**, 1426–1435.

MORRIS, N. A., BUTTSWORTH, D. R., BRESCIANINI, C. P. & JONES, T. V. 1995 An experimental and computational study of moderately underexpanded rocket exhaust plumes in a co-flowing hypersonic free stream. *AIAA Paper* 95-6127.

PAPAMOSCHOU, D. 1991 Structure of the compressible turbulent shear layer. *AIAA J.* **29**, 680–681.

PAPAMOSCHOU, D. & ROSHKO, A. 1988 The compressible turbulent shear layer: an experimental study. *J. Fluid Mech.* **197**, 453–477.

RAGAB, S. A. & WU, J. L. 1989 Linear instabilities in two-dimensional compressible mixing layers. *Phys. Fluids* A **1**, 957–966.

SAMIMY, M. & ELLIOTT, G. S. 1990 Effects of compressibility on the characteristics of free shear layers. *AIAA J.* **28**, 439–445.

SAMIMY, M., REEDER, M. F. & ELLIOTT, G. S. 1990 Compressibility effects on large structures in free shear flows. *Phys. Fluids* A **4**, 1251–1258.

SANDHAM, N. D. & REYNOLDS, W. C. 1990 Compressible mixing layer: linear theory and direct simulation. *AIAA J.* **28**, 618–624.

SHAU, Y. R. & DOLLING, D. S. 1992 Exploratory study of turbulent structure of a compressible shear layer using fluctuating Pitot pressure measurements. *Exps. Fluids* **12**, 293–306.

STOLLERY, J. L. 1967 Heat transfer at hypersonic speeds – a survey of recent and current experiments in the imperial college hypersonic gun tunnel. Aeronautical Research Council, ARC 29 611, HMT 166.

TANG, W., KOMERATH, N. M. & SANKAR, L. N. 1990 Numerical simulation of the growth of instabilities in supersonic free shear layers. *J. Propulsion Power* **6**, 455–460.

WHITE, F. M. 1991 *Viscous Fluid Flow*, 2nd edn., p. 514. McGraw-Hill.

ZHUANG, M., KUBOTA, T. & DIMOTAKAS, P. E. 1988 On the instability of inviscid, compressible free shear layers. *AIAA Paper* 88-3538.